Ocean Engineering 236 (2021) 109441

Contents lists available at ScienceDirect

Ocean Engineering

journal homepage: www.elsevier.com/locate/oceaneng

Dynamic analysis of two-rotor wind turbine on spar-type floating platform

Omar El Beshbichi *, Yihan Xing, Muk Chen Ong

Department of Mechanical and Structural Engineering and Materials Science, University of Stavanger, Stavanger, Norway

ARTICLE INFO

Keywords:
Floating offshore wind turbines
Dynamic analysis
Multi rotor wind turbines
Spar-buoy platform
Modelica

ABSTRACT

The dynamic response of a two-rotor wind turbine mounted on a spar-type floating platform is studied. The response is compared against the baseline OC3 single-rotor design. Structural design shows how the two-rotor design may lead to a mass saving of about 26% with respect to an equivalent single-rotor configuration. Simulations predict significant platform yaw response of the two-rotor floating wind turbine — about 6 deg standard deviation at the rated operating wind speed. It is shown how the platform yaw response is directly caused by the turbulence intensity at the hub coupled with the transversal distribution of thrust loads on the structure. A coupled control strategy for the rotor-collective blade pitch controller is proposed, in which a simple proportional control mitigating platform yaw motion is superimposed to the baseline OC3 PI controller. Numerical simulations show how platform yaw response is reduced by about 60%, at the cost of mean power loss at below-rated wind speeds of about 100 kW and maximum increase of the rotor-collective blade-pitch angles standard deviation of about 2 deg. Parametric analysis of mooring lines design shows how an equivalent mass density of the line of at least 190 kg/m is needed to avoid vertical loads at the anchors.

1. Introduction

Offshore wind energy is a steadily growing industry, reaching in 2019 a total worldwide offshore wind power capacity of 30 GW out of a total worldwide wind power capacity of 600 GW (GWEC, 2019). Offshore wind energy is appealing since wind speed is much greater offshore than inland, and since many of the drawbacks of wind turbine deployment derives from interaction with populated areas (Cruz and Atcheson, 2016). Ideal wind energy sites are mostly locations where water depth far exceeds 50 m, while bottom-fixed offshore wind turbines are economically feasible to be deployed only in shallow water depths (Jonkman, 2007). Floating wind turbines (FOWTs), able to be deployed in deep waters, offer a technological solution, and may thus help in the reduction of the overall levelized cost of energy (LCoE) associated with wind energy.

Reduction of the overall LCoE may in principle be achieved also by means of downscaling wind turbines into equivalent multi-rotor systems (two or more wind turbines installed on the same structure). The development of multi-rotor wind turbines is an old idea, first developed early in the 20th century when the lack of advanced glass fiber composite materials made the manufacturing of large rotors unfeasible (Jamieson and Branney, 2012). The rated power of a wind turbine is proportional to the net area swept by the rotor blades — it thus scales with the square of the rotor radius. However, the blade mass generally increases with the cube of the rotor radius, thus making an array of smaller turbine units advantageous (Jamieson and Branney, 2012). Multi-rotor wind turbine concepts are also interesting from an economical and logistical perspective, since small blades are easier to manufacture, transport, and deploy with respect to state of the art blade sizes. Vestas Wind Systems A/S installed a multi-rotor demonstrator at the Technical University of Denmark, named 4R-V29, composed of four 225kW wind turbines mounted on a single structure and in operation between 2016 and 2019. van der Laan et al. (2019) recently compared numerical results obtained from several Reynolds-Averaged Navier–Stokes equations (RANS) tools against field measurements of power performance and wake deficit, showing faster wake recovery and marginally higher power output at below-rated environmental conditions given by the rotors aerodynamic interaction. Bastankhah et al. (Bastankhah and Abkar, 2019) also performed a large-eddy simulation to study the wake flow properties of a similar four-rotor concept. They found out that the wake recovery is faster at short downwind distances with respect to a single-rotor system. The EU-funded project InnWind (Jamieson et al., 2015) proposed a 20 MW configuration composed of 45 turbines 444 KW each. Conclusions claimed a reduction of the LCoE against an equivalent single-rotor configuration of about 15%. Kirchner-Bossi and Porté-Agel (2020) showed that the optimization of the layout of multi-rotor wind farms may lead to significant benefits also in terms of overall power density compared to a baseline single-rotor wind farm layout. Research of multi-rotor concepts mounted on

* Corresponding author.
E-mail address: omar.elbeshbichi@uis.no (O. El Beshbichi).

https://doi.org/10.1016/j.oceaneng.2021.109441
Received 25 November 2020; Received in revised form 30 June 2021; Accepted 2 July 2021
Available online 13 July 2021

floating platforms is to date scant. First concepts date back to the time of the earliest works in the field, such as the work of Heronemus (1972). Multiple Unit Floating Offshore Windfarm (MUFOW) (Barltrop, 1993) was a UK based project started in 1993 aiming at the investigation of the feasibility of arrays of wind turbines mounted on a single floating platform. However, the idea has yet to be studied thoroughly and its feasibility has yet to be analyzed in detail. The overall dynamic response of the floating system must be carefully studied, as well as the aerodynamic interaction of the rotors under operative and extreme environmental conditions.

In this work, the dynamic response of a two-rotor wind turbine mounted on a spar floating platform is studied. The study relies upon a reduced aerodynamic model, simplified yet adequate to get the overall dynamic characteristics of the multi-rotor FOWT concept. The advantageous stability and relatively simple design and manufacturing of spar-type platforms made it one of the most studied designs over the years, and the abundance of reference designs makes it suitable to be used in conceptual analyses. Phase IV OC3, for instance, is widely used as a major reference design (Jonkman, 2010, 2009a). Full-scale deployment of floating wind turbines also utilized spar-type design, as in Hywind Demo (Equinor, 2020a), the first full-scale prototype of a FOWT deployed in Norway in 2009, as well as in Hywind Scotland (Equinor, 2020b), the first floating wind farm situated in Scotland and commissioned in 2017.

The analysis of this work relies on an in-house tool for the simplified fully-coupled analysis of FOWTs concepts. The predictive tool is developed in Modelica, a non-proprietary, declarative, object-oriented language developed by the non-profit Modelica Association and employed to conveniently model multi-domain systems (The Modelica Association, 2020). The multi-rotor FOWT system is modeled as a rigid body. A dummy degree of freedom (DOF) describing the simplified rigid rotor dynamics is added to the system equations of motion (EQM) in order to determine the aerodynamic state of the system. The aerodynamic loads are then modeled as concentrated thrusts acting on the rotor hubs and as concentrated torques acting on the rotor low-speed shafts. The aerodynamic loads are computed by considering the relative velocity between the hub and wind transversal to the rotor plane and mapping the steady-state aerodynamic coefficients of the wind turbine. This method is thought of as a simplified alternative to more complex beam-element/momentum (BEM) models, and previous work (El Beshbichi et al., 2021) showed how results obtained are accurate in terms of overall dynamic response in operative environmental conditions. The method, however, presents major limitations when considering more complex dynamic interactions. The rotors flexibility and dynamic contributions to the overall system dynamics are neglected. The aerodynamic interaction between rotors, as well as the aerodynamic effects induced by skewed flows are also not considered.

The present work is structured as follows. First, the two-rotor wind turbine concept (2WT) is presented. A simple structural study is carried out in order to define first-attempt tower dimensions and inertial properties. Moreover, the spar platform design is carried out by setting forth general hydrostatic performance considerations. Next, the dynamic response of the 2WT system is analyzed and contrasted with the response of the reference OC3 floating wind turbine. The response of the 2WT system is analyzed by means of two different rotor-collective blade pitch control strategies: the baseline OC3 controller, and a coupled controller that incorporates mitigation of yaw response. Finally, remarks about mooring lines dimensioning applied to the 2WT system are given.

2. Multi-rotor wind turbine concept

Fig. 1 shows the multi-rotor wind turbine concept defined in the present work in relation to the standard OC3 design (Jonkman, 2007, 2010). The concept is composed of a two-rotor wind turbine mounted on a spar-buoy floating platform. As in any new technology development, the multi-rotor FWT will eventually converge to the most optimal concept. This means that the OC3 spar design might not be the most optimal concept for the multi-rotor WT. However, the OC3 spar design has been studied extensively by a large number of researchers over the last decade. Using this concept in the present paper offers the advantage of greatly aiding result assessment.

Table 1
NREL offshore 5-MW Baseline Wind Turbine Specifications (Jonkman, 2007).

Rotor Diameter	m	126
Hub Height	m	90
Rotor Mass	kg	110×10^3
Nacelle Mass	kg	240×10^3
Cut-In, Rated, Cut-Out Wind Speed	m/s	3, 11.4, 25
Cut-In, Rated Rotor Speed	rpm	6.9, 12.1

Table 2
Parameters used in simple tower structural design (Eurocode 3, 2006).

ρ_{steel}	kg/m^3	8500
S_{yield} (JIS SS400)	MPa	230
Wire Grade, R_r	MPa	1960
Wire Fill factor, f	–	0.8
Wire Spinning loss factor, k	–	0.9
Wire Self weight	N/mm^3	830×10^{-7}
Safety factor, γ	–	1.4

The hub height from the sea water level (SWL) is about 90 m, while the horizontal distance between the hubs is about 138.6 m. The center of gravity (COG) of the OC3 system is about 78 m from the SWL, while it is about 100.9 m for the 2WT system. Standard NREL 5-MW wind turbines are used in this study, whose main specifications are listed in Table 1. The horizontal rotor spacing is assumed to be 10% of the rotor diameter, inspired by the multi-rotor turbine concept installed at DTU Risø by Vestas A/S (Bastankhah and Abkar, 2019). The 2WT tower is composed of a main vertical tapered cylinder, a secondary vertical cylinder mounted on top of it, and two horizontal tapered cylindrical arms supporting the rotor nacelle assemblies (RNAs). Wires are used to connect the end of the horizontal arms to the top of the vertical structure. The inclination angle of the wires is 30 deg. This structural geometry allows for distribution of the aerodynamic loads on the horizontal arms as bending loads, while the wires distribute the static loads given by the arms self-weight and RNAs concentrated weight at the hubs as compression loads on the main structure. The assessment of local buckling resistance is neglected at this stage.

In the context of the present work, a simple structural dimensioning of the tower is carried out with the aim of defining first-attempt global inertia properties of the FOWT system. The following study is thus simplified and not intended to focus on detailed structural design. Table 2 shows the parameters used for the simplified structural design, while Table 3 summarizes the selected tower geometry in terms of cross-sectional dimensions of each tower sub-domain. Data are given in terms of inner diameter, outer diameter, and related thickness, and are given both at the base and top of the sub-structure. Intermediate cross-sections are defined through linear tapering. The structural computation assumes the maximum aerodynamic thrust acting at the hub, i.e., 808kN for the NREL 5-MW wind turbine (Jonkman, 2007). The wire tension and the reaction forces acting at the horizontal arms base are readily computed by solving the associated statically indeterminate beam problem. The loaded cross-section area must be big enough to prevent yield (S_{yield}). Yield assessment is performed at the most stressed sections of the structure, i.e., at the tower base and at the horizontal arm base. A safety factor (γ) of 1.4 is used to obtain a conservative design. The yield assessment can be prescribed as follows:

$$\frac{4 r_{out} M}{\pi ({r_{out}}^4 - {r_{in}}^4)} \leq \frac{S_{yield}}{\gamma} \tag{1}$$

where M is the bending load acting at the base of the tower sub-domain, and r_{out} and r_{in} are the outer and inner radii at the base cross-section, respectively. Maximum and minimum values of thickness are considered, equal to 0.04 m and 0.001 m, respectively. The bending moment acting at the base of the horizontal arms is assumed given by

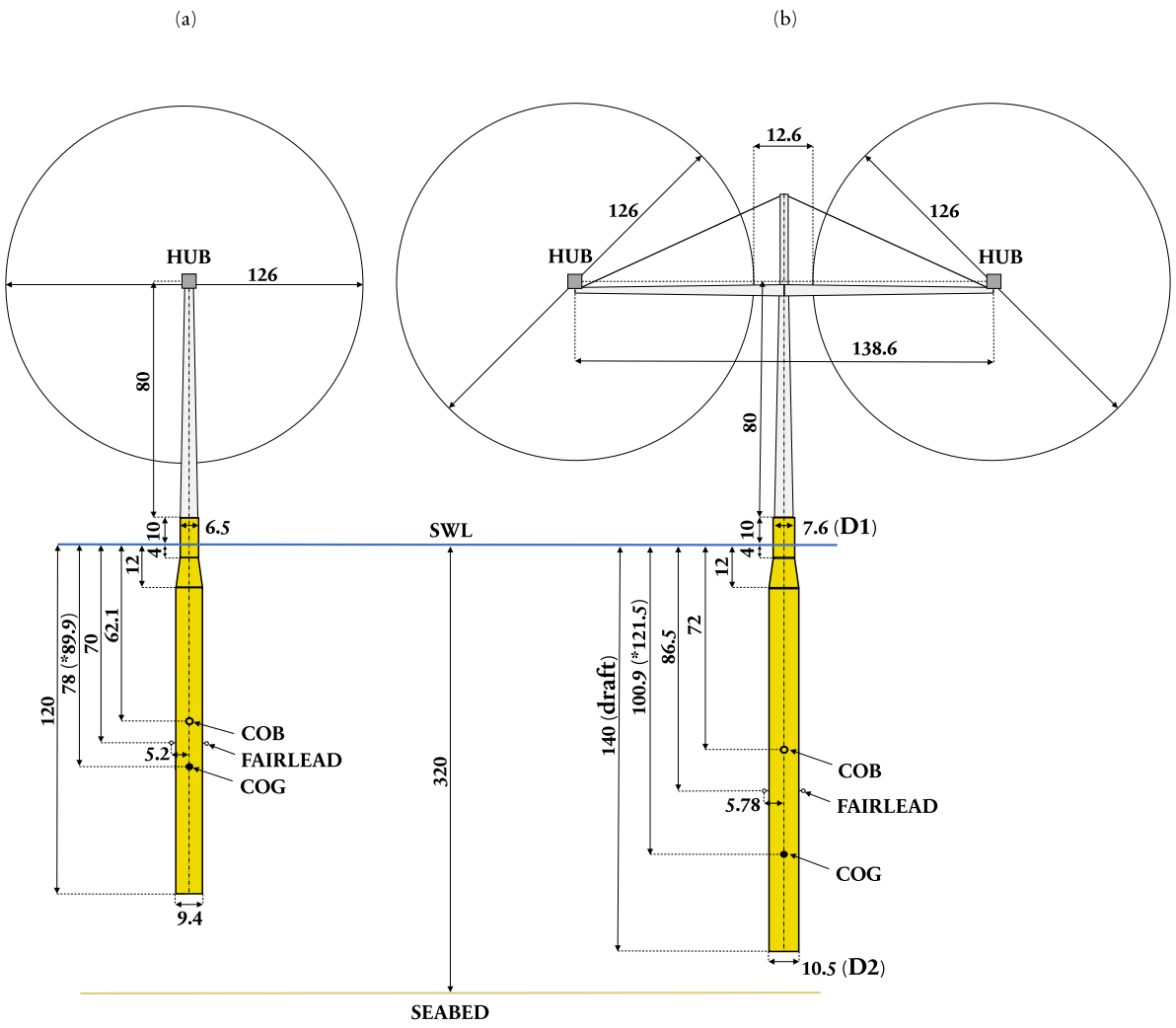

Fig. 1. (a) OC3 geometry [m] (Jonkman, 2007, 2010). (b) 2WT configuration selected in the present study [m]. (* When only the floating platform is considered, the depth to COG is 89.9 m for the OC3 platform, and 121.5 m for the 2WT configuration).

Table 3
Tower geometry selected in simple structural design, maximum loads and utilization ratio.

		Vertical tower	Horizontal arms	Top cylinder	Wire
Inner diameter (base)	m	6.22	4.732	3.26	–
Outer diameter (base)	m	6.28	4.79	3.29	–
Thickness (base)	m	0.03	0.028	0.014	–
Inner diameter (top)	m	4.75	1.79	3.26	–
Outer diameter (top)	m	4.79	1.77	3.29	–
Thickness (top)	m	0.0215	0.014	0.014	–
Diameter	mm	–	–	–	107
Effective load, S_e (bending/axial)	MPa	135	94	–	1058
S_e/S_{yield}	–	0.58	0.40	–	0.54

the action of the aerodynamic thrust, the RNA weight concentrated at the hub, and the horizontal arm self-weight. On the other hand, the bending moment acting at the base of the vertical tower is assumed chiefly related to the action of the aerodynamic thrusts. Effective loads, as well as the ratio between effective and yield stress, are listed in Table 3. The bending stress obtained is equivalent to about 94 MPa at the horizontal arms base and about 135 MPa at the vertical tower base, following an utilization ratio close to 50%. The total concentrated mass of the tower thus defined is about 536.9 tonnes. The wire dimensioning is carried out in accordance with the recommended guidelines of the standard EN1993-1-11 (based on EN 1990) (Eurocode 3, 2006). The wire cross-section must be big enough to prevent yield under maximum external load. A value of γ equal to 1.4 is used also in this case. The wire diameter can be estimated as follows (Eurocode 3, 2006):

$$d_{wire} \geq \sqrt{\frac{4T\gamma}{\pi f k R_r}} \tag{2}$$

where T is the wire tension, R_r is the wire grade, f is the wire fill factor, and k is the spinning loss factor. The obtained wire tension is about 7730kN, while the obtained wire diameter is about 107 mm. The wire concentrated mass is about 4.94 tonnes.

3. Platform design criteria

The dimensioning process of a floating platform is mainly driven by (1) the maximization of pitch stiffness in order to reduce maximum

static pitch angle, (2) the maximization of natural heave period in order to reduce wave-induced motion, and (3) the reduction of the overall cost, chiefly driven by the platform mass and dimensions (Cruz and Atcheson, 2016). Fatigue criteria are also applied in later design stages but may be neglected in conceptual design. The design space of a spar-buoy platform is generally composed of the platform draft, the upper diameter D_1, and the lower diameter D_2 as major design parameters. Platform design parameters associated to the final system geometry adopted in this work are those depicted in Fig. 1. The distance between the SWL and the top of the platform is equal to the value used in the standard OC3 design, that is, 10 m. The distance between SWL and the top of the lower spar section is also equal to the standard OC3 value, 12 m. Spar thickness is assumed constant and equal to 0.05 m. The platform design is carried out in terms of hydrostatic performance, and simple computations can at this stage be employed in order to obtain useful predictions. The following sections present a brief discussion of the common criteria used in platform design.

3.1. Hydrostatic considerations

The major criteria used in platform design can be described as follows:

1. The floating platform must achieve hydrostatic equilibrium. In order to enforce the constraint, the mass of the spar-buoy ballast is imposed by means of the following hydrostatic vertical equilibrium:

$$m_{ballast} = \frac{\rho_{water} V_w g - 3F_{m,v} - m_s g - m_{t,n,r} g}{g} \tag{3}$$

where ρ_{water} is the water density, V_w is the water displaced volume, g is the acceleration due to gravity, $F_{m,v}$ is the total vertical mooring line static load, m_s is the spar-buoy mass, and $m_{t,n,r}$ is the mass of tower, nacelles, and rotors. In the design process, the ballast center of gravity is assumed to be located at 5 m from the bottom of the spar-buoy platform. $F_{m,v}$ is assumed equal to the vertical mooring line static load of the OC3 standard design.

2. The maximum static pitch angle must be sufficiently small, in order to avoid an excessive pitch dynamic response and to limit the loss of annual energy production (AEP) due to the skewed flow conditions (Cruz and Atcheson, 2016). According to Zambrano et al. (2006), the maximum static pitch angle must not exceed 5 deg with ±15 deg of dynamic amplitude. The static pitch angle can be estimated as follows (Pham and Shin, 2019):

$$\theta_5 = \frac{F_{thrust} HB}{C_{55}} \tag{4}$$

where θ_5 is the static pitch angle, F_{thrust} is the overall thrust force acting at the hubs, HB is the vertical distance from the hubs to the center of buoyancy (COB) of the spar-buoy platform, and C_{55} is the hydrostatic restoring pitch stiffness, which can be derived from metacentric height relationships (Faltinsen, 1993).

3. The pitch and heave natural periods must be larger than 25–30 s in order to avoid resonance motions with first-order wave effects (Bachynski and Moan, 2012). The heave period is estimated as follows:

$$T_{33} = 2\pi\sqrt{\frac{m_{tot} + A_{33}}{\rho_{water} g A_w}} \tag{5}$$

where m_{tot} is the overall FOWT mass, A_{33} is the added mass component in heave direction, and A_w is the waterplane area. The value used to estimate A_{33} is assumed in the design stage constant and equal to the value associated with the standard OC3 platform (Jonkman, 2010). The pitch period is estimated by considering surge–pitch coupling. The estimation is carried out by solving the associated surge–pitch characteristic equation:

$$\left(-\omega^2\left(\begin{bmatrix} m_{tot} & z_{cog} m_{tot} \\ z_{cog} m_{tot} & I_{55} \end{bmatrix} + \begin{bmatrix} A_{11} & A_{15} \\ A_{51} & A_{55} \end{bmatrix}\right) + \left(\begin{bmatrix} 0 & 0 \\ 0 & C_{55} \end{bmatrix} + \begin{bmatrix} C_{m,11} & C_{m,15} \\ C_{m,51} & C_{m,55} \end{bmatrix}\right)\right)\underline{\phi} = \underline{0} \tag{6}$$

where ω and $\underline{\phi}$ are the eigenvalues and eigenvectors of the system, z_{cog} is the vertical location of the overall center of gravity of the FOWT system, I_{55} is the overall pitch inertia, A_{11}, A_{15}, A_{51}, and A_{55} are, respectively, the added mass in surge, surge–pitch, pitch–surge, and pitch directions, and $C_{m,11}$, $C_{m,15}$, $C_{m,51}$, and $C_{m,55}$ are, respectively, the mooring linear stiffness values in surge, surge–pitch, pitch–surge, and pitch directions. The pitch period is simply computed as:

$$T_{55} = \frac{2\pi}{\omega_5} \tag{7}$$

where ω_5 is the eigenvalue associated with the pitch direction. The values used to estimate the added mass and mooring lines linear stiffness are assumed in the design stage constant and equal to the value associated with the standard OC3 platform (Jonkman, 2010). The mooring lines stiffness is relative to an unstretched length of 902.2 m, a mass density of 77.71 kg/m, a vertical static length of 250 m, and a diameter of 0.09 m. The platform draft affects the vertical static length of the mooring lines, and consequently the mooring lines stiffness. Hence, a difference is to be expected between the dynamic response of the system and the hydrostatic results. The difference is assumed to be small in pitch and heave directions and therefore tolerable in a preliminary design context.

3.1.1. Periods

Fig. 2 shows the variation of heave and pitch periods of the 2WT system as a function of the draft, lower diameter D_2, and higher diameter D_1 within 100 m<draft<170 m, 10 m<D_2<12 m, and D_1 either equal to 7.5 m (left-hand side plots) or equal to 10 m (right-hand side plots). The red dot denotes the final spar design configuration selected in the present work. As shown, the pitch period tends to increase in configurations with shorter draft and D_2 lengths, while it does not vary substantially with variations of D_1. Values obtained indicate that only for unrealistic configurations given by extremely long draft and D_2 the pitch period becomes unacceptably short. The heave period tends to increase in configurations with longer draft and D_2 lengths and reduces substantially in configurations with longer D_1 lengths. Note that in the case of D_1 = 10 m, the heave period reduces to values close to 25 s for feasible values of draft and D_2. Also for this reason, longer D_1 lengths should be avoided.

3.1.2. Maximum static pitch angle

Fig. 3 shows the maximum static pitch angle of the 2WT system as a function of platform design parameters within the same value range used in Fig. 2. As it is clear, a greater maximum static pitch angle is obtained for shorter lengths of draft and D_2. Longer lengths of D_1 reduce to a minor extent the static pitch angle. The isoline relative to 4–5 deg should be considered as a threshold for acceptable platform configurations. Note that the maximum static pitch angle is the most stringent constraint in the design of multi-rotor floating wind turbines, given that it eliminates most of the design space.

3.1.3. Mass sensitivity

Fig. 4 shows the overall spar-buoy mass (including ballast) as a function of platform design parameters within the same value range used in Fig. 2. The spar mass should always be minimized in order to reduce the construction, material, and deployment cost.

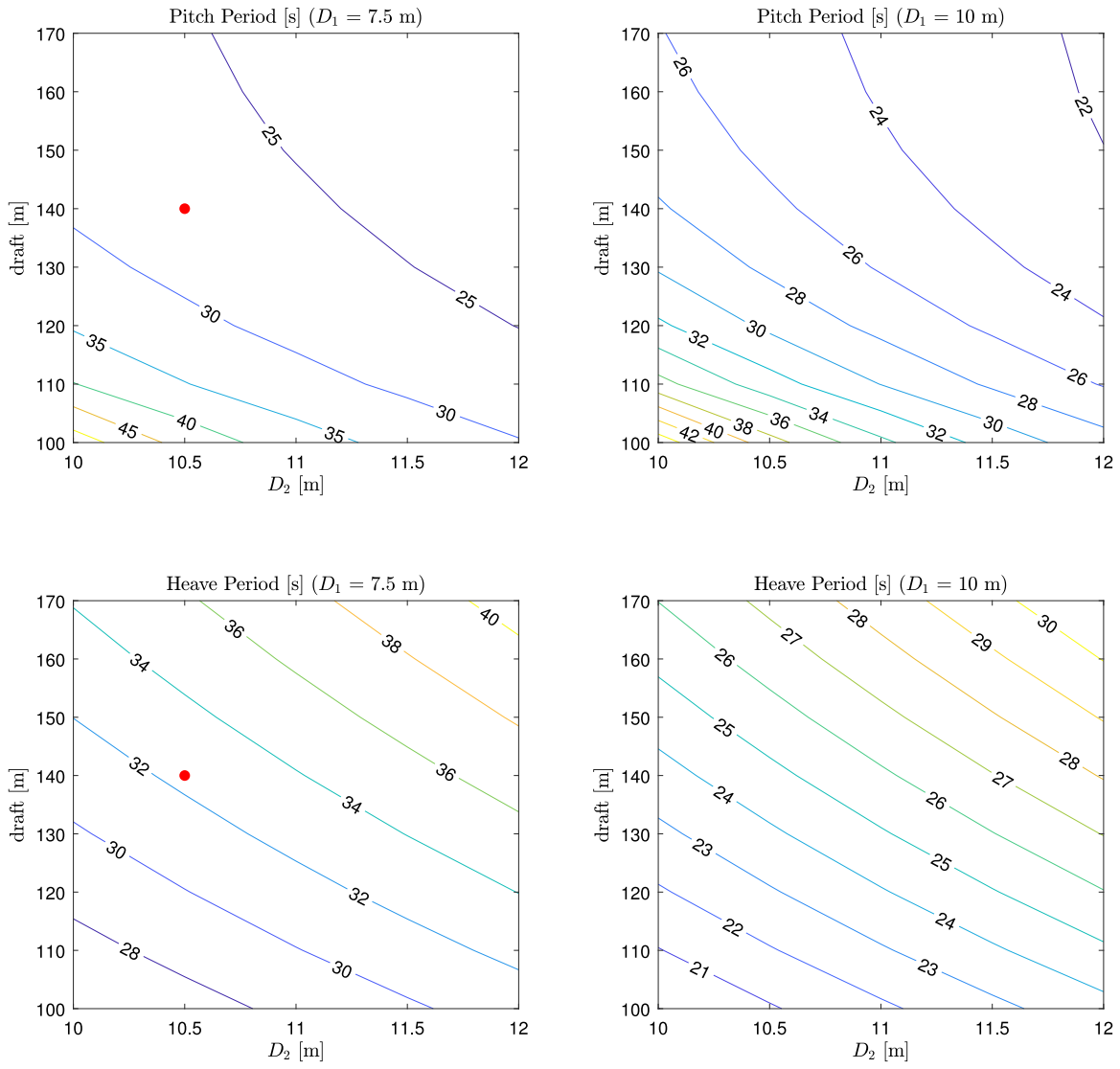

Fig. 2. Pitch and Heave periods as a function of platform design parameters. Left plots are relative to an upper diameter $D_1 = 7.5$ m. Right plots are relative to an upper diameter $D_1 = 10$ m. The red dot denotes the design point selected in this work.

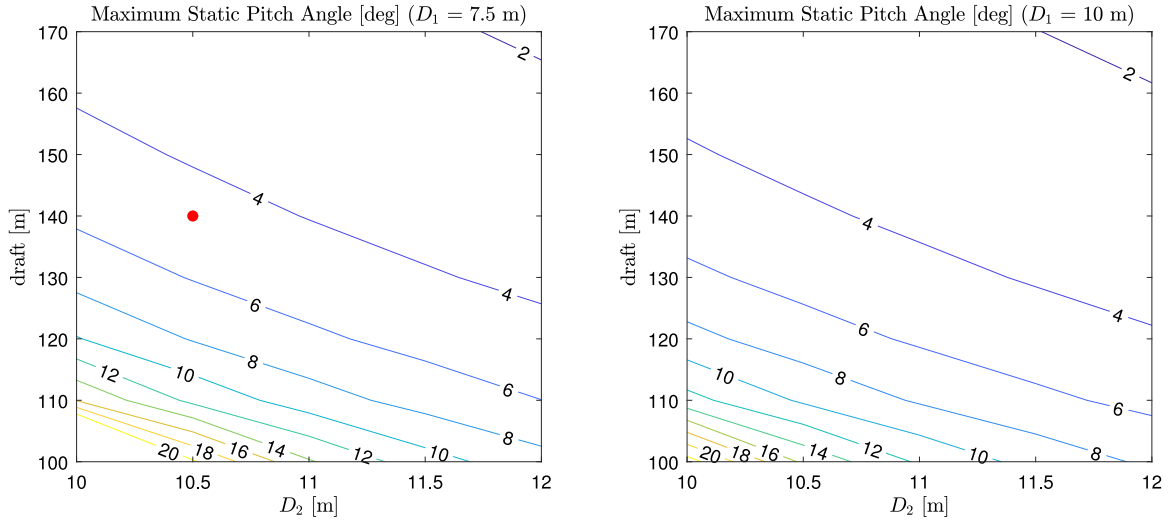

Fig. 3. Maximum static pitch angle as a function of platform design parameters (maximum thrust is assumed). Left plot is relative to an upper diameter $D_1 = 7.5$ m. Right plot is relative to an upper diameter $D_1 = 10$ m. The red dot denotes the design point selected in this work.

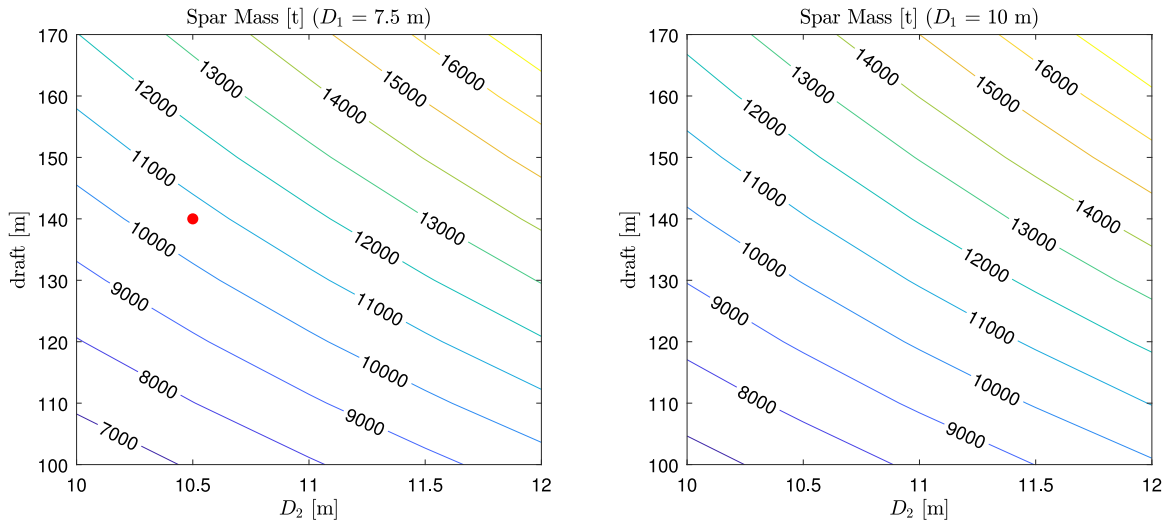

Fig. 4. Overall spar-buoy mass (including ballast) as a function of platform design parameters. Left plot is relative to an upper diameter D_1 = 7.5 m. Right plot is relative to an upper diameter D_1 = 10 m. The red dot denotes the design point selected in this work.

3.2. Platform configuration

The selection process of a feasible platform configuration is based on a trade-off among the design constraints previously mentioned. The main design objective is to achieve acceptable hydrostatic performance and to minimize the platform mass to be employed. Drafts longer than 140 m are unfeasible to deploy and are susceptible to fatigue loading, while higher D_2 lengths generally lead to excessive manufacturing and deployment costs (Cruz and Atcheson, 2016). From design considerations several conclusions can be drawn. For a multi-rotor FOWT employing multi-MW wind turbines, such as the 2WT concept considered in the present study, heave and pitch periods are generally not a stringent constraint within the region of feasible designs in view of the greater inertia involved. For draft lengths shorter than 130–140 m the maximum static pitch angle exceeds the limit imposed of 5 deg. This constraint is the most stringent of the design process. Higher D_1 lengths are slightly beneficial in terms of maximum static pitch angle, but significantly reduce the heave period and increase the platform mass of about 500 tonnes. In the present work, the platform configuration selected is characterized by a draft of 140 m, D_1 = 7.5 m, and D_2 = 10.5 m. Table 4 summarizes the geometrical, the inertial, and the hydrostatic specifications of the configuration selected, together with the specifications of the baseline OC3 spar-buoy platform. The fairlead depth from SWL is assumed to be equally distanced from the COG and the COB, as in the case of the baseline OC3 design. The fairleads depth from SWL is thus equal to 86.5 m. The ratio between the fairlead radius and D_2 is set equal to the one used in the baseline OC3 design. The fairlead radius from the centerline is thus equal to 5.78 m. The overall concentrated mass of the 2WT system is about 11.8×10^3 tonnes. The moments of inertia are computed by employing a CAD model of the FOWT system. The RNA mass is assumed to be concentrated at the hub. The associated inertia tensor of the 2WT system computed at the COG can be written as follows:

$$[I]_{2WT} = \begin{bmatrix} 6.13 \times 10^{10} & -5.93 \times 10^{5} & 1.67 \times 10^{7} \\ -5.93 \times 10^{5} & 5.77 \times 10^{10} & 1.47 \times 10^{5} \\ 1.67 \times 10^{7} & 1.47 \times 10^{5} & 3.69 \times 10^{9} \end{bmatrix} \text{kgm}^2 \tag{8}$$

Table 5 shows the relative variation of mass between two standard OC3 wind turbine units and an equivalent 2WT concept. Even without performing structural optimization, the present 2WT design brings about a significant mass saving of about 26.3% with respect to an equivalent single-rotor configuration. Equivalently, the rated power-to-weight ratio associated to the 2WT concept is about 0.85 W/kg, in place of 0.61 W/kg of the OC3-Hywind design. However, the power-to-weight ratio does not consider the overall power performance of the system but assumes rated power for each rotor as independent systems. The aerodynamic performance of the 2WT design must be carefully studied by considering all the major aerodynamic effects and interactions before an accurate statement on power performance can be drawn.

Table 4
Geometrical–inertial–hydrostatic specifications for the platform configuration selected in the present work and for the standard OC3 spar platform (Jonkman, 2007).

		OC3	2WT
D_1	m	6.5	7.6
D_2	m	9.4	10.5
draft	m	120	140
Depth to COG	m	89.92	121.5
Water Displacement	m^3	8×10^3	11.7×10^3
Mass (including ballast)	kg	7.4×10^6	10.6×10^6
Roll Moment of Inertia about COG	kgm^2	4.2×10^9	1.13×10^{10}
Pitch Moment of Inertia about COG	kgm^2	4.2×10^9	1.13×10^{10}
Yaw Moment of Inertia about Centerline	kgm^2	1.6×10^8	1.7×10^8
Heave Hydrostatic restoring stiffness	N/m	3.3×10^5	4.56×10^5
Roll Hydrostatic restoring stiffness	Nm/rad	1.3×10^9	3.42×10^9
Pitch Hydrostatic restoring stiffness	Nm/rad	1.3×10^9	3.42×10^9
Mass (platform, ballast, tower, nacelle, rotor)	kg	8.06×10^6	11.8×10^6

Table 5
Mass saving between two OC3 units and a single 2WT concept.

		2-OC3	2WT	Variation
Mass (platform, ballast, tower, nacelle, rotor)	kg	16.12×10^6	11.8×10^6	−26.30%

4. Fully-coupled dynamic analysis

In this work, the coupled dynamic behavior of the 2WT concept is studied by employing an in-house code implemented by means of the object-oriented language Modelica. The approach allows for easy implementation of arbitrary platform geometries and platform/rotor configurations. Previous benchmarking work (El Beshbichi et al., 2021) based on the International Energy Agency (IEA) code-to-code comparisons for the baseline OC3 design (Jonkman et al., 2010) has also shown how this method gives good agreement to well established dynamic codes in situations where rotor dynamic contribution can be neglected. The system is assumed to be rigid. The hydrodynamic added damping values employed are assumed equal to those associated with

Table 6
Load cases (LCs) (Bachynski and Moan, 2012).

Case		1	2	3
Significant wave height, H_s	m	2.5	3.1	4.4
Peak wave period, T_p	s	9.8	10.1	10.6
Mean wind speed at hub, U	m/s	8	11.4	18
Turbulence intensity at hub, I	–	0.20	0.17	0.15

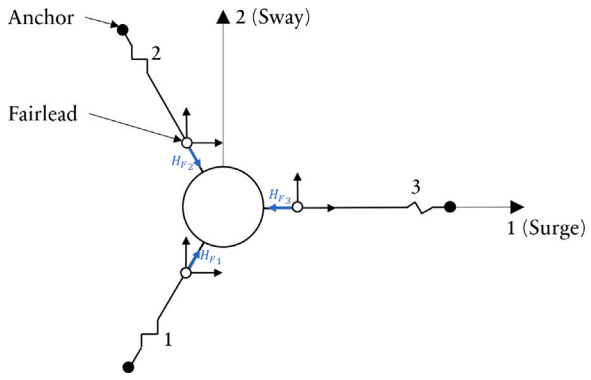

Fig. 5. Mooring lines schematization (top-view) (El Beshbichi et al., 2021).

the baseline OC3 design. Albeit yaw mooring stiffness is associated with the mooring lines design, in this work its value is assumed constant and equal to the one characterizing the baseline OC3 design. The rotor inertial effects, including the contribution of gyroscopic effects on the system dynamics, are not considered.

4.1. Environmental conditions

Three specific load cases (LCs) are considered in this work. Each case is characterized by directionally congruent turbulent wind and irregular waves based on standard JONSWAP spectra. Table 6 summarizes the characteristics of the LCs selected. The cases considered are relative to different environmental severity regions. The first case (LC1) is relative to a below-rated operational wind speed, the second case (LC2) is relative to the rated operational wind speed, and the last case (LC3) is relative to above-rated operational wind speed. Wave energy content increases accordingly. The turbulence intensity at the hub follows the Kaimal spectrum with IEC Class B normal turbulence model (NTM), based on the standard IEC 61400-1 (IEC, 2005).

4.2. Hydrodynamic modeling

The hydrodynamic loads are computed from linear (Airy) wave theory. Airy theory can be applied if the water depth is sufficiently deep (DNV-GL, 2010). The numerical-panel code Sesam-Wadam (DNV-GL) (DNV-GL, 2020) is used to solve the frequency-domain linear hydrodynamic problem relative to the selected platform geometry. Time realizations of irregular wave loads are preventively computed by means of Inverse Fourier Transformations (IFT). The additional load contribution associated with hydrodynamic viscous drag is not considered in this work ($C_d = 0$). However, it should be noted that viscous drag loads may be significant in extreme environmental situations where much larger waves and current effects are considered (Zheng et al., 2020).

4.3. Mooring lines modeling

Mooring lines design is assumed in this work equal to the standard OC3 design, that is, three catenary mooring lines mounted at 120 deg from one another (Jonkman, 2010). Fig. 5 shows a top-view schematization of the standard mooring system employed in the 2WT spar-buoy platform, based on the OC3 design. $H_{F,1,2,3}$ are the horizontal mooring loads acting at the fairleads. Even though the delta catenary mooring lines used in the OC3-Hywind platform are not subject to significant yaw moments, their designs allow for yaw stiffness, which may be easily increased by increasing the fairlead length. A quasi-static formulation of the mooring lines loads is employed in order to obtain the loads–displacements relationship at the fairleads (Jonkman, 2007). The effect of the mooring lines design on the yaw stiffness is neglected, and a constant equivalent yaw stiffness of 9.8×10^7 Nm/rad is used throughout the results to account for the effect of the delta lines. Moreover, the OC3-Hywind load–displacement relationship in the platform's yaw direction is found to be linear at least up to a platform's yaw angle of about 20 deg (Jonkman, 2010). A linear stiffness relationship can then be used also where the platform's yaw motion is considered significant. The mooring lines mass density used is set in this work equal to 200 kg/m.

4.4. Aerodynamic modeling

In this work, the aerodynamic loads are computed by mapping the steady-state thrust and torque aerodynamic coefficients of each rotor. This approach is different to standard codes where a full BEM method is employed, and to simplified codes where the aerodynamic thrust is simply computed as function of the wind speed (Karimirad and Moan, 2012). Integrated loads are used, and hence the distribution of the local aerodynamic loads and the associated local moments on the blades is neglected (Karimirad and Moan, 2012). A simplified rigid rotor EQM is considered to emulate the rotors aerodynamic response. Aerodynamic concentrated thrusts are applied at the hubs, while aerodynamic concentrated torques are applied at the equivalent low-speed rotor shafts. The relative velocity between hub and wind speed transversal to the rotor plane is used. The thrust loads are computed as (El Beshbichi et al., 2021):

$$F = \frac{1}{2}\rho_{air} C_t(\lambda, \beta) A U_{rel}{}^2 \tag{9}$$

where ρ_{air} is the air density, C_t is the steady-state thrust coefficient, λ is the tip speed ratio, β is the rotor-collective blade pitch angle, A is the rotor plane area, and U_{rel} is the relative speed between local wind and hub. The torque loads are computed as:

$$T = \frac{1}{2}\rho_{air} R C_q(\lambda, \beta) A U_{rel}{}^2 \tag{10}$$

where R is the rotor radius, and C_q is the steady-state torque coefficient. The three-dimensional wind velocity profiles at the hubs are computed in Jonkman (2009b) and imported in the code. A 15X15 grid is used, wide enough to encompass the rotors space, and a time step of 0.05 s is used to generate the wind profiles. Wind time histories of 4000 s are computed for each environmental condition. This method, although generating accurate overall dynamic predictions in operational environmental conditions, is not able to detect more complex aerodynamic effects. For instance, the wind profile time realizations used for the computation of the concentrated aerodynamic loads are associated only with the hub locations. This assumption neglects the spatial turbulence variation on the rotors swept area. The effect of the horizontal arms on the local wind induction factors is also not considered. Moreover, skewed blade aerodynamics is not considered, as well as the aerodynamic interaction between the rotors. Albeit literature on similar multi-rotor FOWTs is scant, research works in different fields concerning similar applications, such as the study of thrust deficit induced by the aerodynamic interaction among rotors of Unmanned Aerial Vehicles (UAVs) (Zhou et al., 2017; Alvarez and Ning, 2017), suggest that the effect of the rotor aerodynamic interaction on the overall system response may not be significant enough to compromise the general dynamic behavior obtained in the present study. At any rate, the significance of these effects on multi-rotor FOWT system dynamics can be quantified by employing corrected BEM aerodynamic capabilities in Modelica, which is a task currently under development.

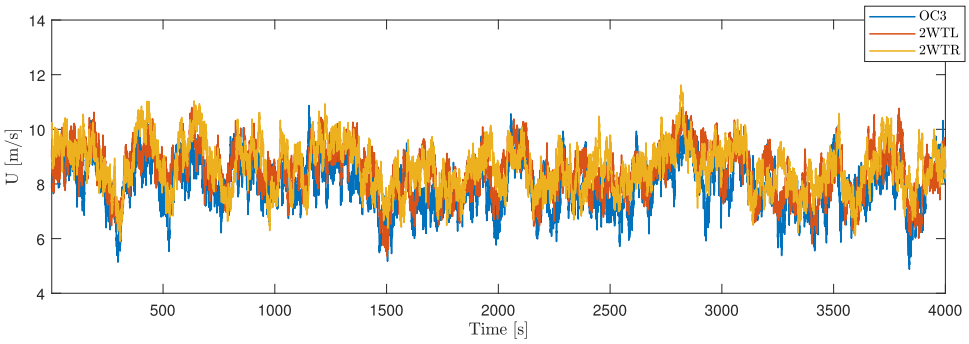

Fig. 6. Wind profiles at the OC3, 2WT left turbine, and 2WT right turbine hub locations relative to the same realization (LC1 — Kaimal turbulence spectrum IEC Class B NTM).

The tower base local reference frame is assumed placed at the same inertial location for all configurations. Fig. 6 shows the wind profiles relative to the same realization and attributed to the hub locations for the OC3 wind turbine, the 2WT left wind turbine (2WTL), and the 2WT right wind turbine (2WTR). The time histories are relative to a mean wind speed of 8 m/s (LC1).

4.5. Control modeling

As it will be presented in detail in Section 5.4, the platform yaw motion response of the 2WT is particularly critical. For this reason, the quantification of the feasibility of mitigating the platform yaw motion by means of an optimized rotor-collective blade pitch control strategy is proposed. The pitch actuator dynamics is assumed fast enough to be neglected for rigid dynamics analysis. That is, there is no delay between the reference pitch angle and the actual pitch angle. A second-order low-pass filter can generally be used to represent pitch actuator dynamics. Common values for cut-off frequency and damping ratio are about 1 Hz and 0.7, respectively — fast compared to the system dynamics (Dunne and Pao, 2016). Two rotor-collective blade pitch control strategies are separately applied to the 2WT concept. The controls employed are the following:

- *OC3 baseline control.* The standard OC3 PI rotor-collective blade pitch control on the generator speed as described in Jonkman (2007) is used to independently control both rotors.
- *Coupled control.* The baseline OC3 baseline PI rotor-collective blade pitch control on the generator speed is linearly coupled with a proportional rotor-collective blade pitch control on the 2WT platform yaw motion.

The coupled control strategy proposed is designed to induce a reduction of aerodynamic thrust at the hub whose surge motion brought about by the yaw dynamics is positive. The rotor-collective blade pitch angle, β_i, where i denotes either the left (L) or the right (R) wind turbine, can be computed as:

$$\beta_i(t) = K_P\beta_i(t)\big(\omega_{i,gen}(t) - \omega_{gen,ref}\big) + K_I\beta_i(t)\int_0^t \big(\omega_{i,gen}(t) - \omega_{gen,ref}\big)dt + K_{q6,i}q_6(t)|q_6(t)| \tag{11}$$

where $K_P(\beta)$ and $K_I(\beta)$ are, respectively, the proportional and integral gain-scheduling laws for the baseline OC3-Hywind PI control on the generator speed, $\omega_{gen}(t)$ is the generator speed, $\omega_{gen,ref}$ is the reference (rated) generator speed, $q_6(t)$ is the platform yaw motion in radians, and $K_{q6}(q_6)$ is the proportional gain-scheduling law for the P control on the platform yaw motion, which can be expressed as:

$$\begin{cases} \text{if } i = L \begin{cases} K_{q6,i} = 0, & \text{if } q_6 > 0 \\ K_{q6,i} = K_{P,q6}, & \text{if } q_6 < 0 \end{cases} \\ \text{if } i = R \begin{cases} K_{q6,i} = K_{P,q6}, & \text{if } q_6 > 0 \\ K_{q6,i} = 0, & \text{if } q_6 < 0 \end{cases} \end{cases} \tag{12}$$

where $K_{P,q6}$ is the constant gain to be determined from tuning analysis.

Fig. 7 shows the block diagram representation of the coupled control strategy. Yaw motion is positive if counterclockwise. When the left rotor is considered, the yaw P control contribution is active only if yaw motion is negative. On the other hand, the right rotor yaw P control contribution is active only if the yaw motion is positive. The absolute value of the yaw control contribution is used to compute the final rotor-collective blade pitch angle induced by yaw dynamics. The standard OC3 variable-speed generator-torque control, as well as saturations of the rotor-collective blade pitch angles and pitch rates are also enforced in both cases (Jonkman, 2007). While the PI control on the generator speed is only active if the generator rotational speed reaches rated values, the P control on yaw motion is always activated.

Table 7 summarizes the control gains used in this work. As it will be described in detail in Section 5.2, a constant gain for the yaw control equal to 1.5 is selected. Fig. 8 shows a time history of about 500 s of the rotor-collective blade pitch angle dynamics and thrust forces for both wind turbines of the 2WT concept with coupled control. The control dynamic response is associated to above-rated environmental conditions (LC3 - Table 6). The plot also shows the associated yaw response. The effect of the linear coupling between the baseline OC3 PI control and the yaw P control is clearly noticeable, as well as the associated influence on the rotor thrusts.

5. Results

The integration method *dassl* is employed to solve the equations of motion of the system, with a tolerance equal to 1×10^{-6} and a time step equal to 0.1 s. A simulation time equal to 4000 s is carried out. The first 400 s are discarded in order to let the initial transients of the system die out. The effective time series used to compute results are thus about 1-h long. Three systems are tested under the same environmental conditions: the baseline OC3 design, the 2WT concept with OC3 baseline control, and the same 2WT system with coupled control as described in Section 4.5. Every system employs mooring lines with a mass density of 200 kg/m. The dynamic response results are given in terms of platform motion q, upstream fairlead tension T_2, and electric power production P_e, and are expressed in terms of overall mean values, μ, and standard deviations, σ.

5.1. System natural periods

Table 8 summarizes the damped natural frequencies of the 2WT system as computed from free decay tests in Modelica. The results obtained are compared against the damped natural frequencies of the OC3 system when the mooring mass density is equivalent to either the one used in the 2WT system (200 kg/m) or to the standard value found in the literature (77.7 kg/m) (Jonkman, 2007). The yaw stiffness of the OC3 system is assumed constant in the two cases. The assumption is reflected in a constant OC3 yaw period for different mooring characteristics. Higher inertia involved in the 2WT system lead to significantly

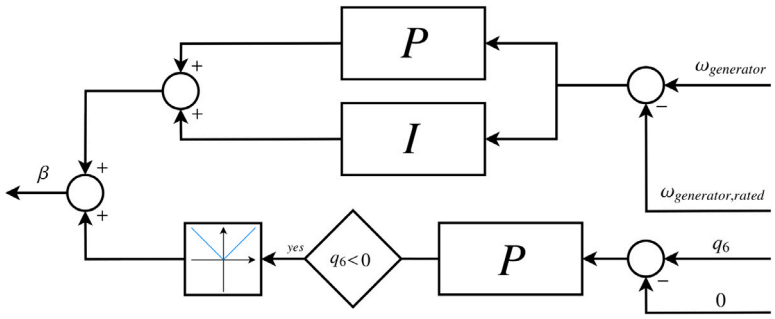

Fig. 7. Block diagram of the 2WT coupled control concept for left wind turbine (right wind turbine condition: $q_6 > 0$).

Table 7
Control systems specifications (Jonkman, 2010).

Proportional Gain at Minimum Blade-Pitch Setting (Generator speed control)	–	0.00627
Integral Gain at Minimum Blade-Pitch Setting (Generator speed control)	–	0.00089
Generator Torque at Rated Speed	Nm	43093
Proportional Gain (2WT yaw motion control)	–	1.5

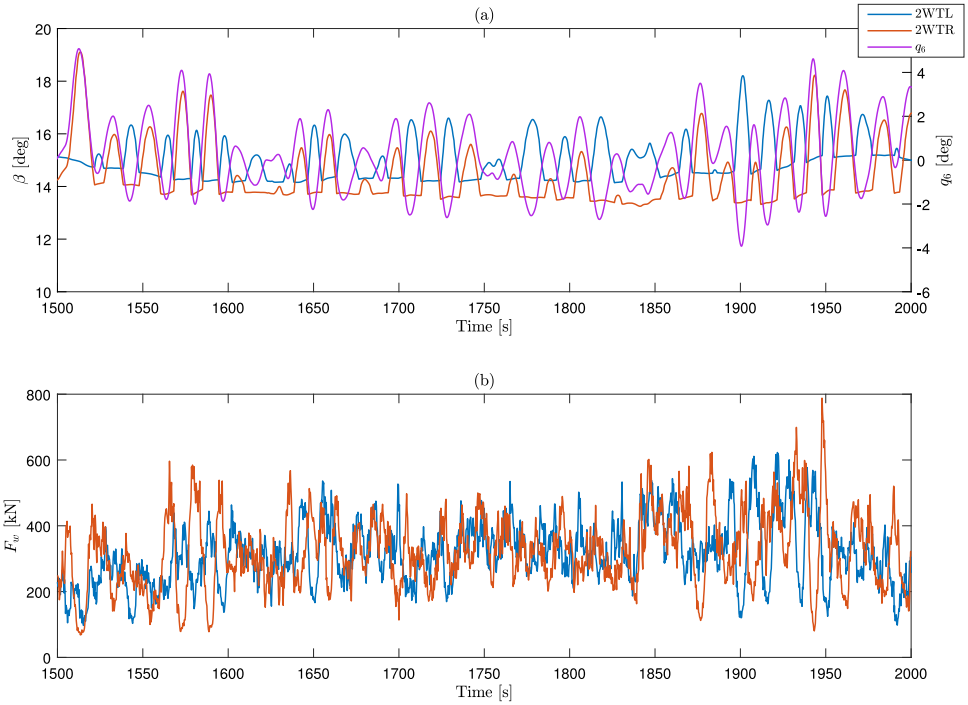

Fig. 8. (a) Rotor-collective blade pitch angles and platform yaw motion. (b) Aerodynamic thrusts at hub. Coupled control schedule for 2WT at above-rated environmental condition (LC3).

Table 8
2WT and OC3 damped natural periods, obtained from free decay tests in Modelica (note that mooring line mass density and yaw stiffness used with 2WT system are 200 kg/m and 9.8×10^7 Nm/rad, respectively Jonkman, 2007).

		2WT	OC3 (200 kg/m)	OC3 (77.7 kg/m)
Surge	s	132.3	103.1	123.45
Heave	s	32.1	30.9	31.8
Pitch	s	29.7	28.2	28.5
Yaw	s	33.6	8	8.19

higher surge and yaw periods with respect to the OC3 system. As expected from preliminary hydrostatic considerations, 2WT heave and pitch periods are for this configuration sufficiently longer than the limit imposed to avoid first-order wave excitations.

5.2. Effect of yaw control proportional gain tuning (coupled control)

Generally, the tuning process of PI/PID wind turbine controllers is first obtained using methods such as pole-placement or Ziegler–Nichols and then refined by the employment of fully-coupled aeroelastic simulations to obtain an optimized tuning in terms of loads reduction and motion regulation (Ziegler and Nichols, 1993; Mirzaei et al., 2016). On this line, Hansen et al. (2005) determined the gains of a standard rotor-collective blade pitch PI controller by employing a minimization of the blade root flapwise bending moments. Tibaldi et al. (2012) performed a fine-tuning of two PI controllers respectively associated with below-rated and above-rated environmental conditions by minimizing a cost function based on fatigue loads, ultimate loads, annual energy production, and blade pitch actuator duty cycle. Control gain tuning is hence

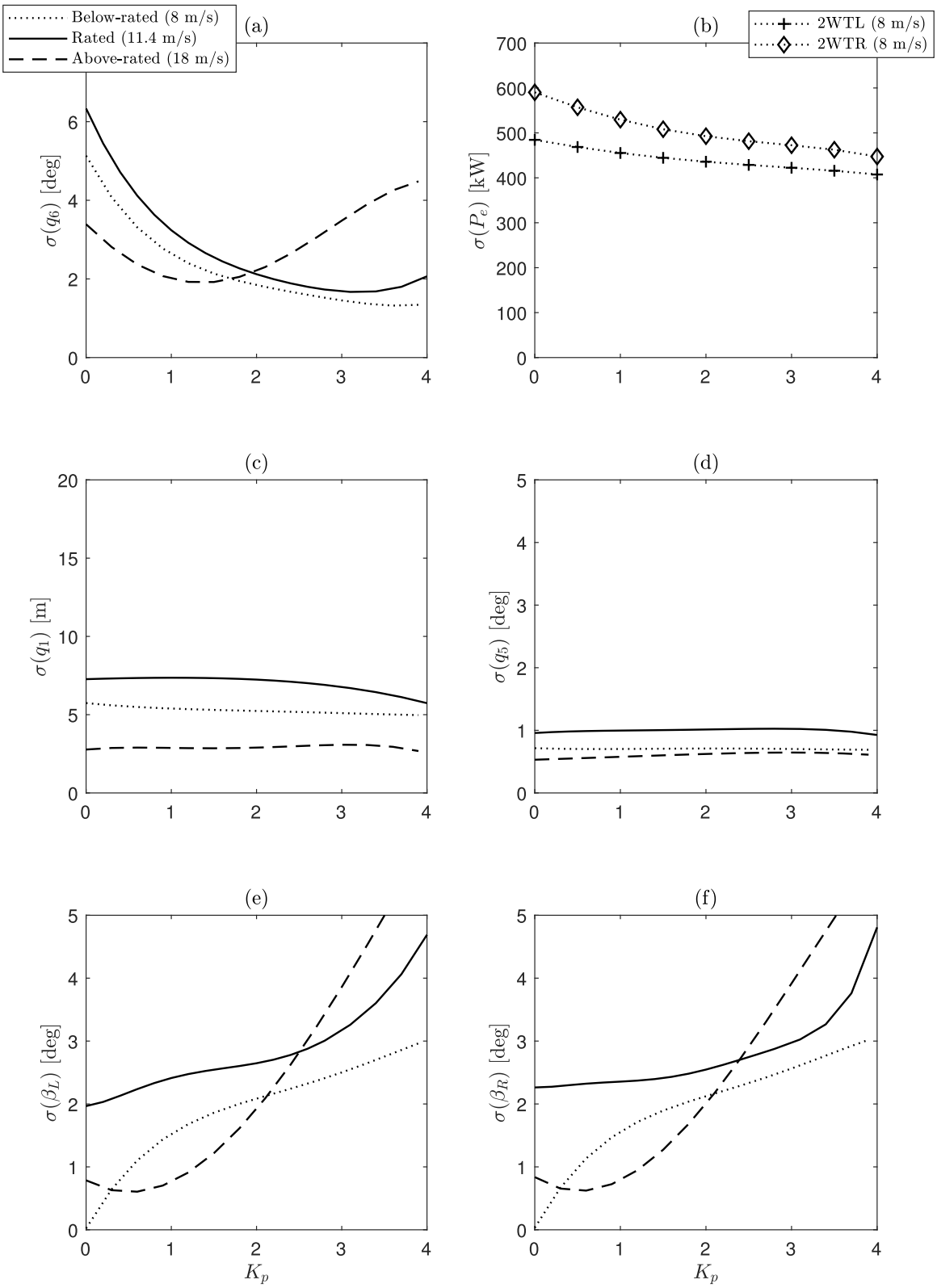

Fig. 9. Standard deviation of (a) platform yaw motion, (b) electric power output, (c) platform surge motion, (d) platform pitch motion, (e) left rotor-collective blade pitch angle, and (f) right rotor-collective blade pitch angle of the 2WT system in relation to the yaw control proportional gain and under different operating wind speed (Table 6).

a trade-off analysis, necessary in order to identify the best tuning setup under contrasting objectives.

The main goal of the current analysis is to quantify the capability of a coupled control strategy to mitigate the platform yaw motion of the 2WT system. For this reason, a simple proportional control of the platform yaw motion is linearly superimposed to the OC3 baseline rotor-collective blade pitch PI control, as presented in Section 4.5. The tuning process is only focused on the additional proportional gain K_p, while the baseline PI controller retains the original OC3 gain-scheduling (Jonkman, 2007). The study of more advanced controllers,

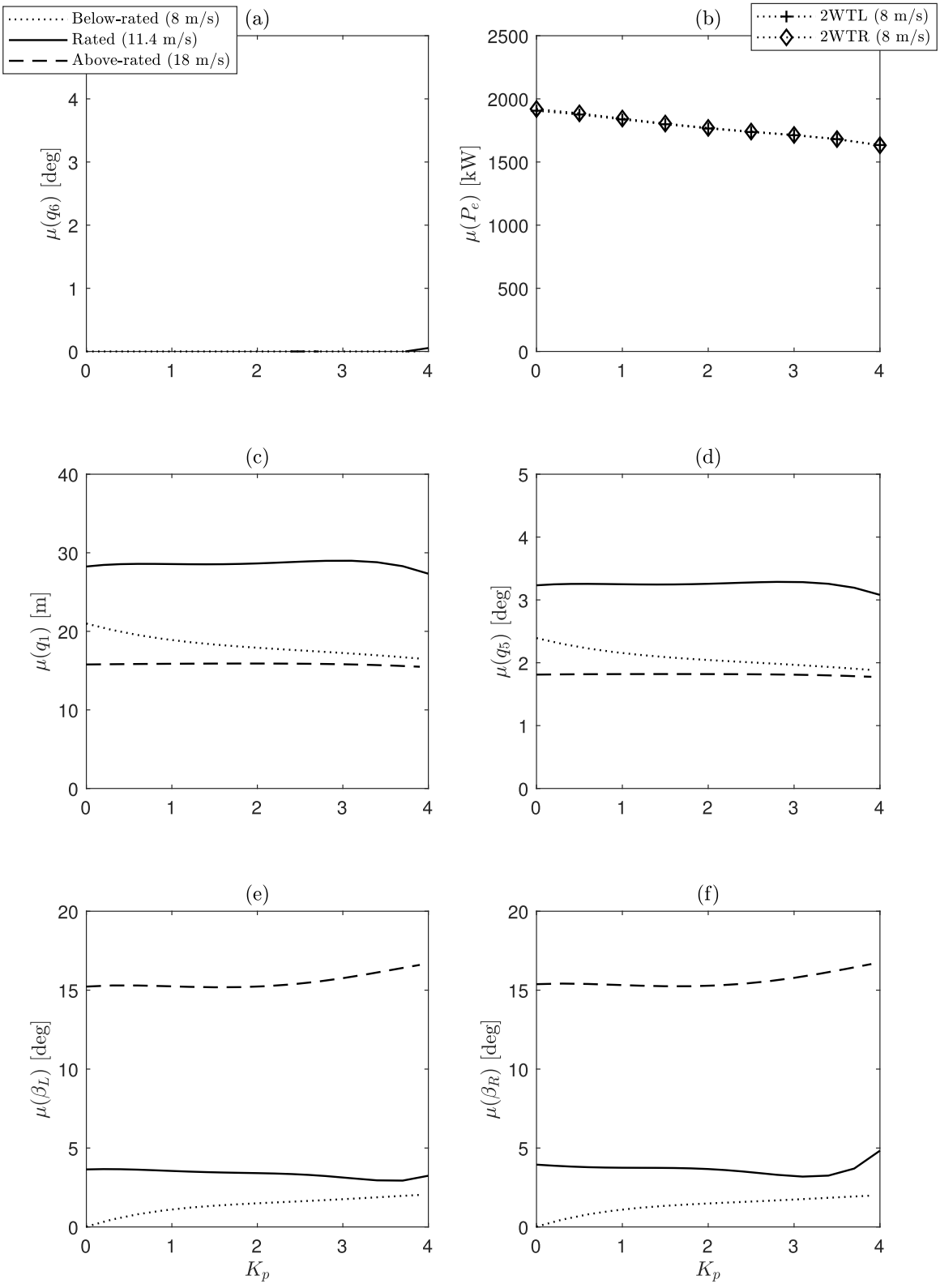

Fig. 10. Mean of (a) platform yaw motion, (b) electric power output, (c) platform surge motion, (d) platform pitch motion, (e) left rotor-collective blade pitch angle, and (f) right rotor-collective blade pitch angle of the 2WT system in relation to the yaw control proportional gain and under different operating wind speed (Table 6).

as well as the study of more thorough tuning strategies being able to further optimize the system response, are left as questions for further research.

The tuning is performed heuristically, and the main drivers are the following: (1) the minimization of platform yaw standard deviation, (2) the maximization of the mean electric power output, and (3) the minimization of the rotor-collective blade pitch angles standard deviation, which can be correlated with the aerodynamic thrust, torque, and the associated blade root loads standard deviation. Fig. 9 illustrates the standard deviations of platform yaw, surge, and pitch motions,

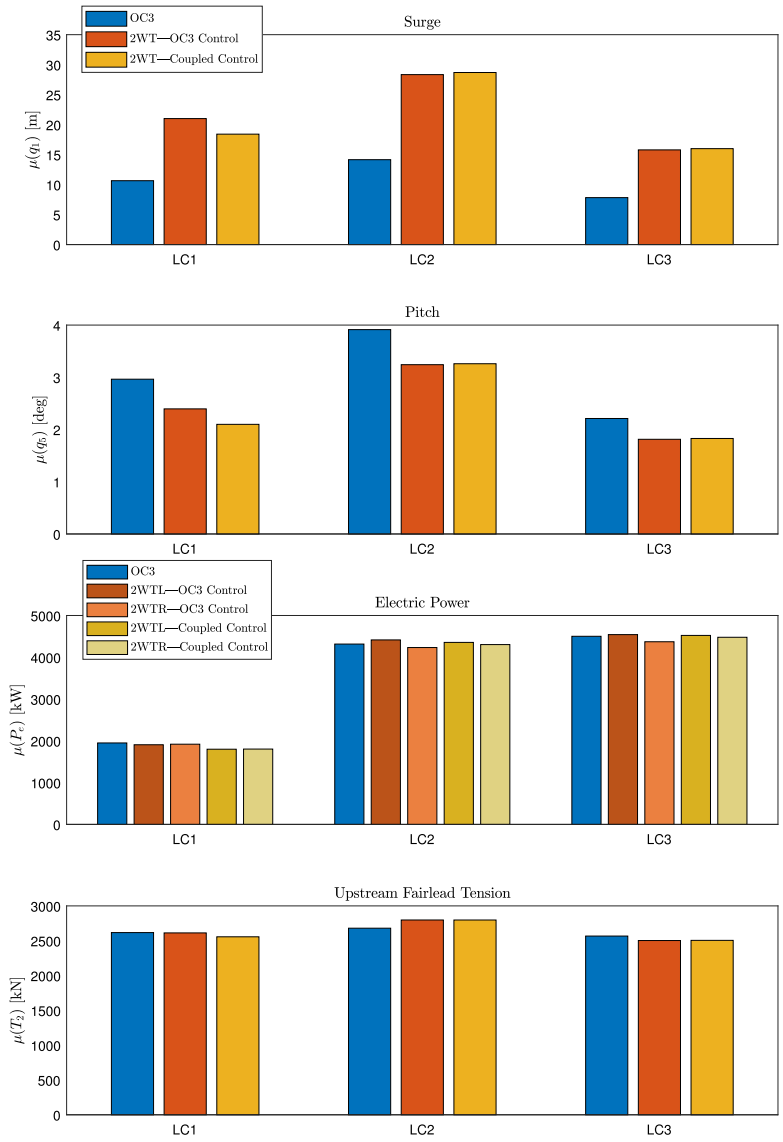

Fig. 11. Mean surge, pitch, electric power production, and upstream fairlead tension (all configurations employ an equivalent mooring line mass density of 200 kg/m).

electric power output, and rotor-collective blade pitch angles of the 2WT system in relation to K_p for below-rated, rated, and above-rated environmental conditions. The platform yaw motion standard deviation reduces significantly for every environmental condition, reaching a minimum region at $K_p \simeq 2$. For above-rated environmental conditions, the yaw motion standard deviation increases significantly at high K_p values due to stalled-induced thrust fluctuations. Platform surge and pitch standard deviations are not notably affected by K_p. It can be noted how the rotor-collective blade pitch angles standard deviation is zero for $K_p = 0$ at below-rated environmental conditions, given by the lack of the PI controller contribution to the system response. The rotor-collective blade pitch angles standard deviation greatly increases with greater values of K_p, showing values higher than 2 deg for $K_p \geq 2$. Fig. 10 illustrates the mean values for the same response parameters used in Fig. 9. Platform surge and pitch mean motion reduces at high K_p values for below-rated environmental conditions, caused by the increased rotor-collective blade pitch mean angle and the associated reduction of aerodynamic thrust. The aerodynamic torque is reduced in the same manner, leading to a reduction of the overall electric power output. For $K_p = 4$ the electric power output loss is about 288kW. As listed in Table 7, the constant yaw control proportional gain selected for the present work is 1.5. Under this tuning schedule, platform yaw motion is minimized at the cost of an electric power output loss of 100 kW for below-rated environmental conditions and the increase of rotor-collective blade pitch angle standard deviation in the range of 0.5–2 deg.

5.3. Dynamic response

Fig. 11 shows the overall mean values for surge and pitch motion, electric power production, and upstream fairlead tension under different load cases for the OC3 system, the 2WT system configured with baseline OC3 control, and the 2WT system configured with the coupled control. Platform sway, heave, and roll motions are found to be small for each system and thus are not depicted in the results. Changing the rotor-collective blade pitch control strategy from the baseline OC3 to the coupled control strategy does not influence significantly the mean response of the 2WT system. As it is clear from the figure, the mean surge values are significantly lower in the OC3 system with respect to the 2WT concept, at each load case about twice the values obtained in the system. This is clearly associated with the doubling of aerodynamic thrust force in the 2WT concept. The maximum surge response in the 2WT concept is about 30 m and is obtained at the rated operating wind speed. The mean pitch values obtained in the OC3 system are higher

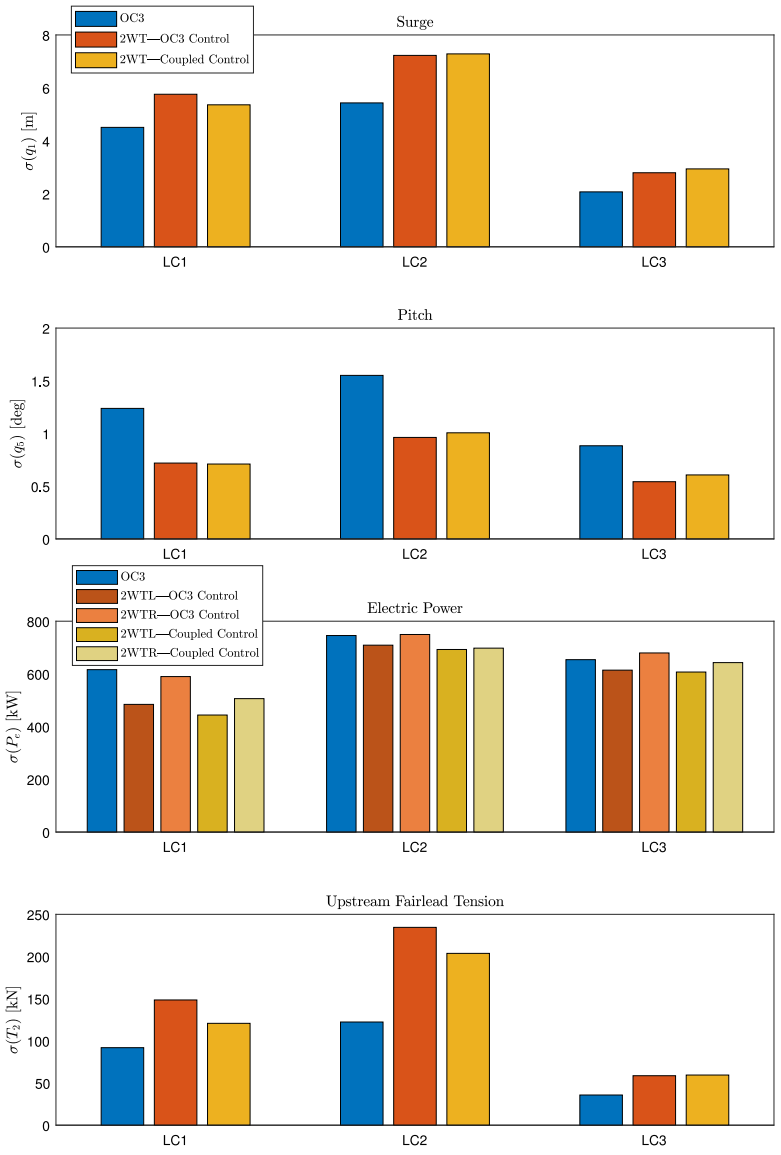

Fig. 12. Standard deviations for surge, pitch, electric power production, and upstream fairlead tension (all configurations employ an equivalent mooring line mass density of 200 kg/m).

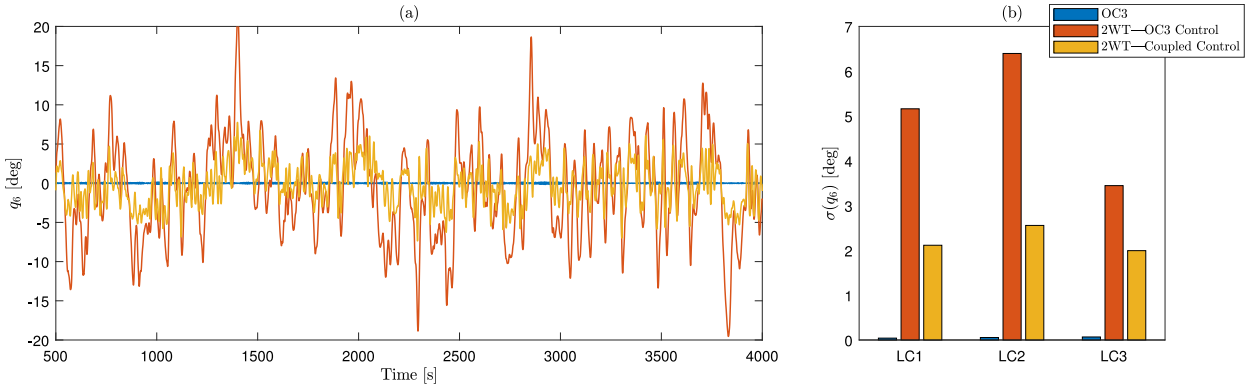

Fig. 13. (a) Time histories for platform yaw motion at the rated operating wind speed (LC2). (b) Standard deviations for platform yaw motion (all configurations employ an equivalent mooring line mass density of 200 kg/m).

with respect to the 2WT concept. The difference is of about 1 deg at the rated operating wind speed. As the pitch angle is one of the floating platform chief design drivers, it may be concluded that some margin is still available to further optimize the platform design. The mean electric power production is broken down into single rotor performance. Since the mean values are computed from single 1-h realizations of turbulent

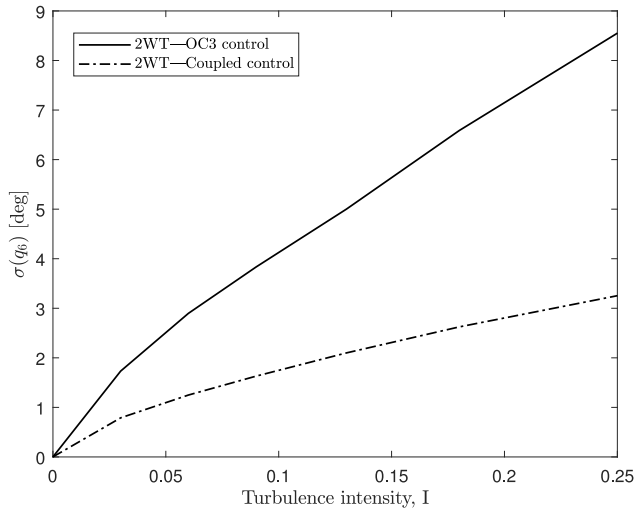

Fig. 14. Standard deviation of platform yaw motion as function of turbulence intensity (11.4 m/s - Kaimal IEC 61400-1 turbulence spectrum).

responses, the mean electric power production for all rotors at rated and above-rated operating wind speed is lower than the rated power of 5 MW (Clifton and Wagner, 2014). This is due to fluctuations of the generator speed in the below-rated region. Moreover, the aerodynamic model employed in this work does not allow for assessment of the contribution of complex aerodynamic effects on the system performance — especially with respect to aerodynamic efficiency and consequently electric power production. Consequently, the mean electric production obtained at below rated speed for the 2WT system with baseline OC3 control is similar to the one obtained in the OC3 system. The interaction effect may be significant and is therefore left at this stage as a question for further research.

Fig. 12 shows the standard deviations for platform surge and pitch motion, electric power production, and upstream fairlead tension for the same load cases and system configurations given in Fig. 11. The pattern obtained is similar to the one characterizing the mean values. Standard deviations obtained for the 2WT system under different control strategies are found to be similar. The electric power production standard deviations associated with the 2WT rotors are found to differ by about 100 kW, particularly at below rated wind speed. The difference is reasonably associated with the different wind velocity profiles at the hub locations. Tension standard deviation is important when evaluating the probability of line slack and fatigue life. In order to avoid slack conditions, the tension standard deviation must be sufficiently smaller than its associated mean value (Bachynski and Moan, 2012). The standard deviation of the upstream fairlead tension for the 2WT system at the rated operating wind speed is significantly higher than in the OC3 system. However, the tension standard deviation is relatively small if compared with its associated mean value (ratio $\sigma/\mu \approx 0.07$), implying that the current mooring layout may be sufficient to withstand survival environmental conditions (Cheng et al., 2017).

5.4. Yaw response

Fig. 13 shows the time histories for the platform yaw motion at the rated operating wind speed (LC2), and the standard deviations for the environmental conditions used in the analysis (see Table 6). The transversal distribution of thrust loads given by the two-rotor configuration significantly affects yaw motion. The response is characterized by long periods. This can be correlated with the concentration of wind turbulence energy in the low-frequency region (Li et al., 2019). The maximum yaw angle in the 2WT concept operating with the baseline OC3 control strategy is about 21.6 deg and it is obtained at the

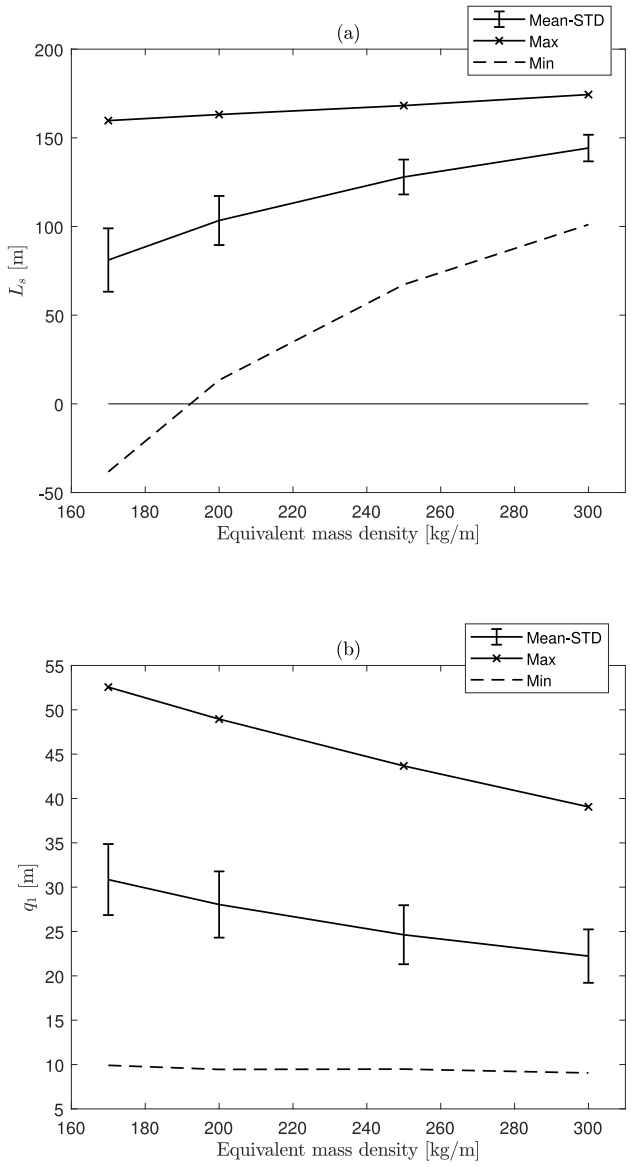

Fig. 15. Effect of mooring line equivalent mass density on the upstream mooring line seabed length (a) and on the platform surge motion (b). Coupled control schedule for 2WT at the rated operating wind speed (LC2).

rated operating wind speed, while the associated standard deviation is about 6.5 deg. The coupled control strategy proposed in this work, albeit simply implementing a proportional control on the platform yaw motion, reduces the overall yaw response of about 60%. The maximum yaw angle at the rated operating wind speed reduces to about 7.7 deg, while the associated standard deviation reduces to about 2.5 deg. The thrust discrepancy at the hubs increases with turbulence intensity, thus increasing the standard deviation of platform yaw motion. Fig. 14 shows the standard deviation for platform yaw motion as a function of the turbulence intensity I, computed at the rated operating wind speed (11.4 m/s). Platform yaw motion is nonlinearly correlated with the wind turbulence level. The significant reduction of the yaw standard deviation in the case the system operates with a coupled control strategy endures at varying turbulence intensities. It is also clear how the standard deviation for platform yaw motion is zero when the wind profile is not turbulent ($\sigma(q_6)|_{I=0} = 0$).

5.5. Mooring configuration

A simple parametric mooring line design of the 2WT system is performed in terms of the effect of the mooring lines equivalent mass density on the system response computed at rated operating wind speed (LC2). The associated findings are illustrated in Fig. 15. The mooring lines diameter is equal to 0.09 m, and the unstretched mooring line length is equal to 902.2 m. For an equivalent mass density of 170 kg/m the peak minimum seabed length is negative, i.e., no portion of the mooring line rests on the seabed and the anchor tension includes a nonzero vertical component. In order to ensure excess mooring line length, an equivalent mass density higher than 190 kg/m is thus necessary. Peak platform surge motion decreases with increasing mooring line weight.

6. Conclusions

The dynamic analysis of a two-rotor wind turbine mounted on a spar-type floating platform has been performed. A simple structural analysis showed how a mass saving of about 26% may be achieved by employing the two-rotor configuration instead of an equivalent single-rotor configuration. The numerical simulations showed an increased low-frequency yaw response of the two-rotor system compared with the response of a single-rotor configuration, of about 6 deg standard deviation at the rated operating wind speed. The yaw excitation is directly induced by the turbulence intensity at the hub and the transversal distribution of thrust loads on the structure. A rotor-collective blade pitch angle coupled control has been proposed for the mitigation of yaw response. The numerical simulations showed a reduction of the yaw response of about 60% at the cost of a reduction of mean power output at below-rated wind speed of about 100 kW. In addition, parametric analysis showed that an equivalent mass density of the mooring lines of at least 190 kg/m is necessary in the 2WT in order to avoid vertical loads at the anchors. Stiffer mooring lines configurations in yaw direction would also reduce platform yaw response. The analysis is based on in-house code developed in Modelica. The aerodynamic model is based on mapping the steady-state aerodynamic coefficients characteristic of the wind turbines employed. The approach is therefore not able to assess complex aerodynamic situations which may be significant. Skewed effects on the aerodynamic efficiency of the blades, especially related to the significant platform yaw angles, cannot be considered to date. Moreover, the aerodynamic interaction between the rotors is not assessed.

Subjects for future work include the study of the aforementioned aerodynamic effects, the study of more advanced strategies for multi-rotor floating wind turbines control, as well as aeroelastic effects and tower structural dynamics interactions. Moreover, the aerodynamic interaction between the rotors should be investigated and included in the dynamic model. Finally, an optimal station-keeping configuration able to maximize yaw stiffness, an optimal platform configuration for multi-rotor applications, as well as fault effects of rotors and control system, should be investigated.

CRediT authorship contribution statement

Omar El Beshbichi: Conceptualization, Methodology, Software, Validation, Formal analysis, Investigation, Writing - original draft, Writing - review & editing, Visualization. **Yihan Xing:** Conceptualization, Methodology, Software, Formal analysis, Investigation, Writing - review & editing, Supervision. **Muk Chen Ong:** Conceptualization, Investigation, Writing - review & editing, Resources, Supervision, Project administration, Funding acquisition.

Declaration of competing interest

The authors declare that they have no known competing financial interests or personal relationships that could have appeared to influence the work reported in this paper.

Acknowledgment

This PhD project is financed by the Equinor Akademia Program at the University of Stavanger, Norway.

References

Alvarez, E., Ning, A., 2017. Modeling multirotor aerodynamic interactions through the vortex particle method. AIAA 2019–2827.
Bachynski, E.E., Moan, T., 2012. Design considerations for tension leg platform wind turbines. Mar. Struct. 29 (1), 89–114.
Barltrop, N., 1993. Multiple unit floating offshore wind farm (MUFOW). Wind Engineering 17 (4), 183–188.
Bastankhah, M., Abkar, M., 2019. Multirotor wind turbine wakes. Phys. Fluids 31 (8).
Cheng, Z., Madsen, H.A., Gao, Z., Moan, T., 2017. Effect of the number of blades on the dynamics of floating straight-bladed vertical axis wind turbines. Renew. Energy 101, 1285–1298.
Clifton, A., Wagner, R., 2014. Accounting for the effect of turbulence on wind turbine power curves. J. Phys. Conf. Ser. 524.
Cruz, J., Atcheson, M., 2016. Floating Offshore Wind Energy - the Next Generation of Wind Energy. Springer.
DNV-GL, 2010. Offshore standard DNV-OS-j101 - design of offshore wind turbine structures.
DNV-GL, 2020. WADAM Official website.
Dunne, F., Pao, L.Y., 2016. Optimal blade pitch control with realistic preview wind measurements. Wind Energy 19 (12), 2153–2169.
El Beshbichi, O., Xing, Y., Ong, M.C., 2021. An object-oriented method for fully coupled analysis of floating offshore wind turbines through mapping of aerodynamic coefficients. Mar. Struct. 78.
Equinor, 2020a. Hywind demo. https://www.equinor.com/en/what-we-do/floating-wind/hywind-demo.html.
Equinor, 2020b. Hywind scotland. https://www.equinor.com/en/what-we-do/floating-wind/hywind-scotland.html.
Eurocode 3, 2006. Design of steel structures - part 1-11: Design of structures with tension components (EN 1993-1-11).
Faltinsen, O.M., 1993. Sea Loads on Ships and Offshore Structures. In: Cambridge Ocean Technology Series.
GWEC, 2019. Global Wind Report.
Hansen, M., Anca, D., Larsen, T., Stig, O., Sorensen, P., Fuglsang, P., 2005. Control design for a pitch-regulated, variable speed wind turbine. In: Risø-R-1500(EN).
Heronemus, W.E., 1972. Pollution-Free Energy from the Offshore Winds. Marine Technology Society.
IEC, 2005. International Electrotechincal Commission, Wind Turbines: Part 1: Design Requirements. Tech. rep. IEC61400-1:2005(E).
Jamieson, P., Branney, M., 2012. Multi-rotors; a solution to 20 MW and beyond? Energy Procedia 24, 52–59.
Jamieson, P., Branney, M., Hart, K., Chaviaropoulos, P.K., Sieros, G., Voutsinas, S., Chasapogiannis, P., Prospathopoulos, J.M., 2015. Innovative turbine concepts - multi-rotor system. In: INNWIND-EU Deliverable 1.33.
Jonkman, J.M., 2007. Dynamics modeling and loads analysis of an offshore floating wind turbine. In: NREL/TP-500–41958.
Jonkman, J.M., 2009a. Dynamics of offshore floating wind turbines-model development and verification. Wind Energy 12 (5), 459–492.
Jonkman, B., 2009b. Turbsim user's guide: version 1.50. In: NREL/TP-500–46198.
Jonkman, J.M., 2010. Definition of the floating system for phase IV of OC3. In: NREL/TP-500–47535.
Jonkman, J.M., Larsen, T., Hansen, A., Nygaard, T., Maus, K., M.Karimirad, Gao, Z., Moan, T., Fylling, I., Nichols, J., Kohlmeier, M., Vergara, J., Merino, D., Shi, W., Park, H., 2010. Offshore code comparison collaboration within IEA wind task 23: phase IV results regarding floating wind turbine modeling. In: European Wind Energy Conference. EWEC.
Karimirad, M., Moan, T., 2012. A simplified method for coupled analysis of floating offshore wind turbines. Mar. Struct. 27 (1), 45–63.
Kirchner-Bossi, N., Porté-Agel, F., 2020. Multi-rotor wind farm layout optimization. J. Phys. Conf. Ser. 1618.
van der Laan, M.P., Garcí a, N., Angelou, N., Pirrung, G., Ott, S., Sørensen, K., Xavier, J., Neto, V., Larsen, G., Mikkelsen, T., Kelly, M., Sjöholm, M., Andersen, S., 2019. Power curve and wake analyses of the vestas multi-rotor demonstrator. Wind Energy Science 4, 251–271.
Li, L., Liu, Y., Gao, Y., 2019. Dynamic and structural performances of offshore floating wind turbines in turbulent wind flow. Ocean Eng. 179, 92–103.
Mirzaei, M., Tibaldi, C., Hansen, M.H., 2016. PI Controller design of a wind turbine: evaluation of the pole-placement method and tuning using constrained optimization. J. Phys. Conf. Ser. 753.
Pham, T.D., Shin, H., 2019. A new conceptual design and dynamic analysis of a spar-type offshore wind turbine combined with a moonpool. Energies 12 (19).
The Modelica Association, 2020. Modelica official website - modelica language.

Tibaldi, C., Hansen, M.H., Henriksen, L.C., 2012. Optimal tuning for a classical wind turbine controller. J. Phys. Conf. Ser. 555.

Zambrano, T., MacCready, T., Kiceniuk, T., Roddier, D.G., Cermelli, C.A., 2006. Dynamic modeling of deepwater offshore wind turbine structures in gulf of mexico storm conditions. In: Volume 1: Offshore Technology; Offshore Wind Energy; Ocean Research Technology; LNG Specialty Symposium, Vol. 1. pp. 629–634.

Zheng, Z., Chen, J., Liang, H., Zhao, Y., Shao, Y., 2020. Hydrodynamic responses of a 6 MW spar-type floating offshore wind turbine in regular waves and uniform current. Fluids 5 (4–187).

Zhou, W., Ning, Z., Li, H., Hu, H., 2017. An experimental investigation on rotor-to-rotor interactions of small UAV. AIAA 2017–3744.

Ziegler, J.G., Nichols, N.B., 1993. Optimum settings for automatic controllers. J. Dyn. Syst. Meas. Control 115 (2B), 220–222.